
**AFRL-AFOSR-JP-TR-2023-0085**

# On-Demand Stoichiometry Control of Copper Sulfide Nanocrystals with Omni-Tunable Semiconductor Properties

**Huh, Wansoo**
**Soongsil University Industry-Academic Cooperat**
**369 Sangdo-ro, Dongjak-gu**
**Seoul, , 06978**
**KR**

**06/23/2023**
**Final Technical Report**



Air Force Research Laboratory
Air Force Office of Scientific Research
Asian Office of Aerospace Research and Development
Unit 45002, APO AP 96338-5002

# REPORT DOCUMENTATION PAGE

**PLEASE DO NOT RETURN YOUR FORM TO THE ABOVE ORGANIZATION.**

| 1. REPORT DATE | 2. REPORT TYPE | 3. DATES COVERED | |
|---|---|---|---|
| 20230623 | Final | START DATE<br>20180808 | END DATE<br>20200807 |

**4. TITLE AND SUBTITLE**
On-Demand Stoichiometry Control of Copper Sulfide Nanocrystals with Omni-Tunable Semiconductor Properties

| 5a. CONTRACT NUMBER | 5b. GRANT NUMBER | 5c. PROGRAM ELEMENT NUMBER |
|---|---|---|
| FA2386-18-1-4008 | | |
| **5d. PROJECT NUMBER** | **5e. TASK NUMBER** | **5f. WORK UNIT NUMBER** |
| | | |

**6. AUTHOR(S)**
Wansoo Huh

**7. PERFORMING ORGANIZATION NAME(S) AND ADDRESS(ES)**
Soongsil University Industry-Academic Cooperat
369 Sangdo-ro, Dongjak-gu
Seoul 06978
KR

**8. PERFORMING ORGANIZATION REPORT NUMBER**

| 9. SPONSORING/MONITORING AGENCY NAME(S) AND ADDRESS(ES) | 10. SPONSOR/MONITOR'S ACRONYM(S) | 11. SPONSOR/MONITOR'S REPORT NUMBER(S) |
|---|---|---|
| AOARD<br>UNIT 45002<br>APO AP 96338-5002 | AFRL/AFOSR IOA | AFRL-AFOSR-JP-TR-2023-0085 |

**12. DISTRIBUTION/AVAILABILITY STATEMENT**
A Distribution Unlimited: PB Public Release

**13. SUPPLEMENTARY NOTES**

**14. ABSTRACT**
The duration of the project was 2 years. electronic properties of electronically coupled copper sulfide nanocrystals Cu2-xS NCs assemblies including their structural, optical, electrical, and thermoelectrical characteristics as a function of atomic stoichiometry of the material were investigated. The electronically coupled assemblies of Cu2-xS NCs in thin films were attained by removing the original long oleic amine ligands employed during the synthetic procedure after assemblies of NCs were formed. Following, the stoichiometric composition or x for the electronically coupled Cu2-xS NCs assemblies was controlled by immersing the solid thin film into a solution containing Cu(I) complex. As Cu gradually incorporated into the copper deficient sites of Cu2-xS NCs, x could be controlled. Consequently, NIR absorbance of the Cu2-xS NC assemblies as well as their electrical conductivity and thermoelectric Seebeck coefficient could be changed systematically with the control in x. Overall, room temperature thermoelectrical power factor as high as 33.1 μW/K2m could be obtained from electronically coupled assemblies of Cu2-xS NCs with x = 0.02.

**15. SUBJECT TERMS**

| 16. SECURITY CLASSIFICATION OF: | | | 17. LIMITATION OF ABSTRACT | 18. NUMBER OF PAGES |
|---|---|---|---|---|
| a. REPORT<br>U | b. ABSTRACT<br>U | c. THIS PAGE<br>U | SAR | 24 |

| 19a. NAME OF RESPONSIBLE PERSON | 19b. PHONE NUMBER *(Include area code)* |
|---|---|
| JEREMY KNOPP | 315-227-7006 |

**Standard Form 298** (Rev.5/2020)
Prescribed by ANSI Std. Z39.18

## TABLE OF CONTENTS

**Section** **Page**

## LIST OF FIGURES

**Page**

## LIST OF TABLES

**Page**

## 1.0 SUMMARY

The hole density of individual copper sulfide nanocrystals ($Cu_{2-x}S$ NCs) is determined from the stoichiometric mismatch ($x$) between copper and sulfide atoms. Consequently, the electronic properties of the material vary over a range of $x$. To exploit $Cu_{2-x}S$ NCs in devices, assemblies of NCs are typically required. The overarching goal of this project is i) to develop an electrochemical platform that allows on-demand control of the stoichiometry for thin film assemblies of $Cu_{2-x}S$ NCs, which, in turn, omni-tunes the physical properties of the films, ii) to investigate fundamental properties of $Cu_{2-x}S$ NCs thin-film assemblies, including electrical conductivity, thermoelectric properties, and optical properties, as a delicate function of charge carrier density, and iii) to provide practical guidelines for utilizing the versatile $Cu_{2-x}S$ NCs in thin-film electronic devices such as light-weight, flexible thermoelectrics.

The stoichiometric control is done by immersing the solid NC assemblies into a solution containing Cu(I) complex for different durations (0–10 min). As $Cu^+$ gradually occupied the copper-deficient sites of $Cu_{2-x}S$ NCs, $x$ could be controlled from 0.9 to less than 0.1. Consequently, the near-infrared (NIR) absorbance of $Cu_{2-x}S$ NC assemblies change systematically with $x$. With increasing $x$, electrical conductivity increased and Seebeck coefficient decreased systematically, leading to the maximal thermoelectric power factor from a film of $Cu_{2-x}S$ NCs at an optimal doping condition yielding $x = 0.1$. The physical characteristics of the $Cu_{2-x}S$ NC assemblies investigated herein will provide guidelines for exploiting this emerging class of nanocrystal system based on doping.

## 2.0 INTRODUCTION

Copper sulfide nanocrystals (NCs) exhibit unique electric/optoelectronic properties due to the stoichiometric mismatch between copper and sulfide atoms. A small amount of copper is thermodynamically driven to escape from the lattice of the crystalline structure, and NCs with copper deficiencies, *i.e.*, $Cu_{2-x}S$ NCs (where $x$ represents the degree of mismatched stoichiometry) are formed.[1-3] Since each copper-deficient site functions as an acceptor to the semiconductor, $Cu_{2-x}S$ NCs yield self-doped *p*-type characteristics, and the hole density changes with $x$. This indicates that the physical characteristics of the material can vary over a range of $x$. For example, $Cu_{2-x}S$ NCs with an abundant number of free holes yield a localized surface plasmon resonance (LSPR) effect in the near-infrared (NIR) regime,[4] which is commonly observed in the visible regime for metallic nanostructures.[5-6] Both the resonant frequency and its intensity change with the number of holes inside the materials and thus with $x$.[7-12] The electrical and thermoelectric properties of bulk $Cu_{2-x}S$ are also functions of hole carrier density,[13-14] indicating that the associated properties of nanostructured $Cu_{2-x}S$ should also vary with $x$. Therefore, methods to finely control the mis-stoichiometry of $Cu_{2-x}S$ NCs, referred as the stoichiometric doping effect, are extensively

considered, and a comprehensive understanding of the resulting physical properties of the materials is critical.

The physical characteristics of NCs exploited in thin film devices are not only determined by the intrinsic properties of NCs alone, but also by the electronic coupling of the materials with each other in assemblies.[15-17] The primary factor governing the coupling between NCs is their inter-distance, which is determined by the ligands surrounding individual NCs.[18-19] Although passivating the surface of NCs with long hydrocarbon ligands (e.g., trioctyl phosphine, oleic acid, or oleylamine) is critical for obtaining a stable colloidal dispersion of NCs, these long insulating ligands typically suppress the electronic coupling between NCs.[20-21] Therefore, the device applications of NC assemblies often require these long ligands to be replaced with short ones in solution or solid films or be completely removed.[19, 22-25] Short amines, thiocyanides, halides, and hydrazine are the common ligands that have been used for such purposes of copper chalcogenide NCs.[8, 26-27] Although studies on the influence of surface ligands on the electronic coupling in $Cu_{2-x}S$ NC assemblies[26] and those on the influence of atomic stoichiometry on the uncoupled $Cu_{2-x}S$ NCs in solution[9, 11] have been conducted separately, the stoichiometric doping on the physical properties of the highly coupled $Cu_{2-x}S$ NC assemblies has been rarely investigated.

## 3.0 METHODS

### 3.1 Chemicals.

Copper(I) chloride (99.995%), sulfur powder (99.98%), oleylamine (technical grade, 70%), sodium sulfide ($Na_2S$), chloroform (anhydrous, ≥99%), hexane (anhydrous, 95%), toluene (anhydrous, 99.8%), ethanol (anhydrous, ≥99.5%), methanol (anhydrous, 99.8%), tetrakiscopper hexafluorophosphate ($Cu(I)(CH_3CN)_4PF_6$, 97%), and ammonium cerium(IV) nitrate ($(NH_4)_2Ce(NO_3)_6$, ≥99.99%) were purchased from Sigma-Aldrich. These chemicals were used as received without further purification.

### 3.2 Synthesis of $Cu_{2-x}S$ NCs.

$Cu_{2-x}S$ NCs were synthesized by modifying a previously described method.[2] Copper(I) chloride (118.8 mg) was added to oleylamine (24 mL) in a three-neck round-bottom flask, followed by degassing. Separately, sulfur powder (48.1 mg) was added to oleylamine (15 mL) in another three-neck round-bottom flask, followed by degassing to form a sulfur precursor solution. The flask containing the sulfur precursor solution was heated at 120 °C under a nitrogen atmosphere for 25 min and then cooled to 40 °C. Meanwhile, the reaction flask with copper(I) chloride was heated at 225 °C under a nitrogen atmosphere until the solution became transparent, then cooled to 125 °C. Subsequently, the sulfur precursor solution (12 mL, 40 °C) was injected into the reaction flask at 125 °C, and the temperature was maintained at 104 °C for 1.5 min to achieve $Cu_{2-x}S$ NC growth.

During the growth, there was a finite variation in the temperature (±3°C). The temperature was then rapidly lowered to room temperature. The resulting NC solution was purified by centrifuging the reaction mixture using ethanol as the anti-solvent to the dispersion twice. Entire precipitation and dispersion processes were done without exposing NCs to ambient condition.

### 3.3 Preparation of electrically coupled assemblies of $Cu_{2-x}S$ NCs.

The substrates (glass, silicon, and silicon with thermally grown silicon oxide (3000 Å)) were cleaned by sonication in acetone and isopropanol in sequence. These substrates were then blown with nitrogen before use. Dispersions of $Cu_{2-x}S$ NCs (20 mg $mL^{-1}$) in hexane:toluene (3:7 volume ratio) were spin-coated (2500 rpm, 60 s) onto the substrates, and the resulting films were annealed at 65 °C for 30 min. $Na_2S$ in ethanol (0.064 M) was dropped onto the $Cu_{2-x}S$ NC film, dwelled for 2 min, then spin-coated at 2500 rpm for 15 s. This time period was sufficient to completely remove the original oleylamine ligands on the surface of the $Cu_{2-x}S$ NCs. The resulting films were rinsed with fresh ethanol, then heated at 80 °C for 3 min using a hot plate. The thin-film formation and ligand removal processes were repeated once more to form fully percolated electronically coupled assemblies of $Cu_{2-x}S$ NCs. All these processes were done inside a nitrogen filled glove box without exposing $Cu_{2-x}S$ NCs to ambient.

### 3.4 Stoichiometric doping on electronically coupled assemblies of $Cu_{2-x}S$ NCs.

Solutions of $Cu(I)(CH_3CN)_4PF_6$ in methanol (1 mM) and $(NH_4)_2Ce(NO_3)_6$ in ethanol (0.4 mM) were prepared separately. The assemblies of $Cu_{2-x}S$ NCs prepared above were dipped into the Cu(I) and Ce (IV) complex solutions for a designated time period. Subsequently, the as-solution-treated $Cu_{2-x}S$ NC film was rinsed with a pristine solvent by gently dripping the solvent onto the film. All these processes were done inside a nitrogen filled glove box without exposing $Cu_{2-x}S$ NCs to ambient.

### 3.5 Characterization of assemblies of $Cu_{2-x}S$ NCs.

TEM was conducted using a Libra 120 (Carl Zeiss) operating at 120 keV. UV-Vis-NIR spectra were obtained using a V-770 UV-Visible/NIR spectrophotometer (Jasco). XRD measurement was performed using an Ultima IV X-ray diffractometer (Rigaku). Electrical conductivity measurements were performed using a four-point probe setup placed inside a nitrogen filled glove box connected to a Keithley 2400 sourcemeter. Thermoelectrical properties were analyzed using a customized measurement stage placed inside a nitrogen filled glove box comprising two Peltier modules, a Keithley 2700 digital multimeter, and a Keithley 2182A nanovoltmeter that was controlled through a LabView code. Thermovoltage was estimated from the slope of the voltage difference and temperature difference plot. XPS measurements were conducted using an AXIS

Ultra DLD (Kratos). FT-IR spectra were obtained using an iS50 FT-IR spectrometer (Thermo Fisher Scientific). AFM measurements were performed using a Park XE7 (Park system).

## 4.0 RESULTS AND DISCUSSION

Two different routes can be designed to obtain electronically coupled $Cu_{2-x}S$ NC assemblies controlled by $x$, because the stoichiometric control of $Cu_{2-x}S$ NCs and the electronic coupling between these NCs require two separate chemical treatment steps. A thin solid film of $Cu_{2-x}S$ NC assemblies is first formed from a dispersion of NCs attached to common long alkyl ligands (Step 1 in **Figure 1**), then the ligands attached to the surface of the NC solid are adjusted to enhance the electronic coupling between the crystals (Step 2 in **Figure 1**). Subsequently, the solid film undergoes chemical treatment for stoichiometric doping to control $x$ (Step 3 in **Figure 1**). Alternatively, the $x$-controlled, electronically coupled $Cu_{2-x}S$ NC assemblies can be prepared by first executing stoichiometric doping of $Cu_{2-x}S$ NCs in solution and then cast the solution as films followed by ligand adjustment (**Figure 2**). From our experiment, reliable results could only be obtained from the first route. When preparing the NC assemblies via the second route, it was challenging to form smooth films for $Cu_{2-x}S$ NCs that had already undergone chemical treatment; this could be owing to the reactants (and products) added to the processing NC dispersion during the doping process. Therefore, the entire dataset provided here is from those obtained from the first route.

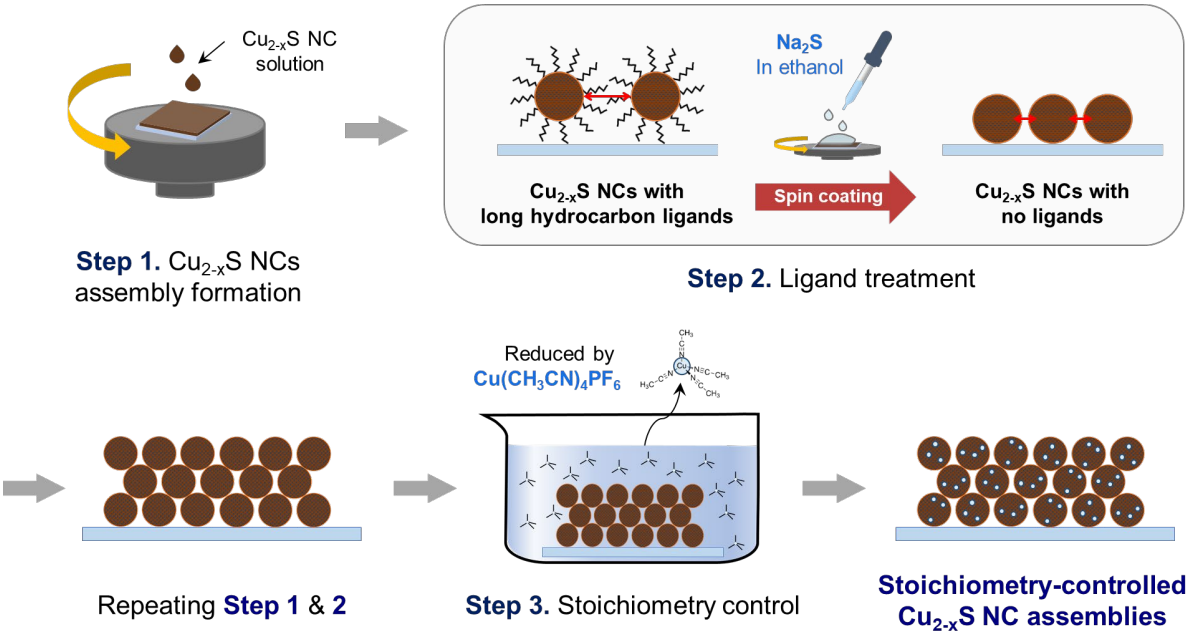


**Figure 1.** Schematic description of attaining electronically coupled $Cu_{2-x}S$ NCs assemblies with control of $x$.

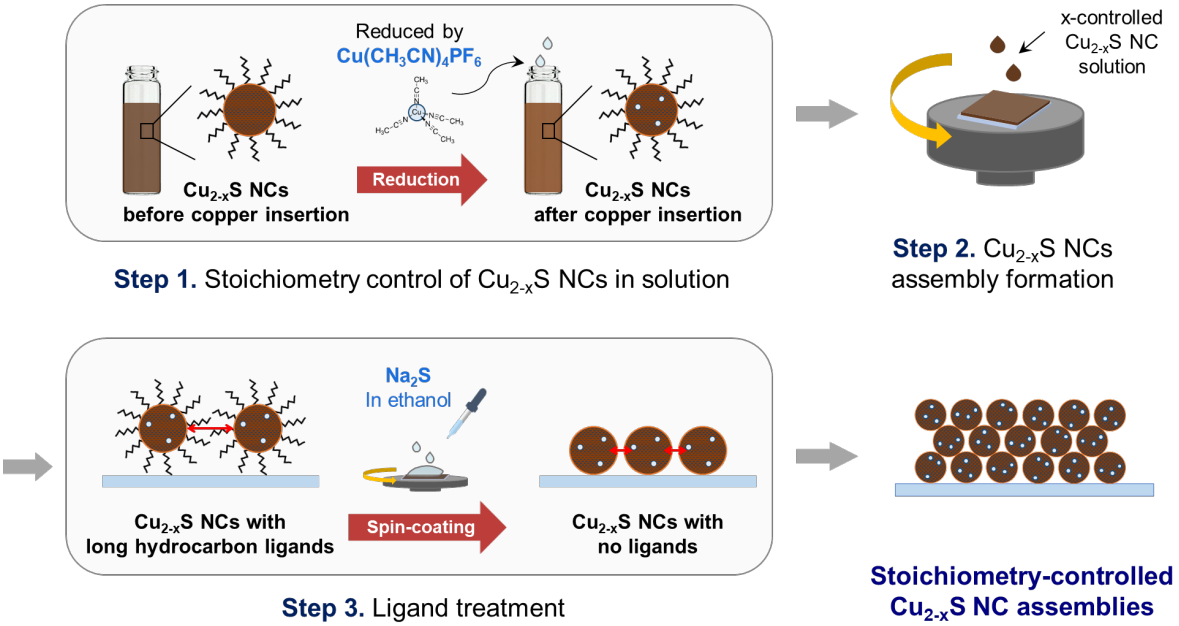


**Figure 2.** Schematic description of attaining electronically coupled $Cu_{2-x}S$ NCs assemblies with control of $x$ in an alternative way.

$Cu_{2-x}S$ NCs were synthesized by a hot injection method according to a modified recipe described previously.[2] **Figure 3a** displays the TEM image of the as-synthesized $Cu_{2-x}S$ NCs passivated with oleylamine. The average diameter of the NCs was 5.5 nm. The relative composition between Cu and S was determined from X-ray photoemission spectroscopy (XPS) measurements, which were found to be 1.1 ($x$ = 0.9). **Figure 3b** shows the diffractogram of the $Cu_{2-x}S$ NCs obtained from XRD measurements. The overall shape of the pattern matched well with that of $Cu_{1.3}S$ NCs from Manna et al.,[11] but a small shift towards a lower 2θ angle was observed. The series of peaks from Manna et al. (blue) is also plotted for comparison; these peaks were ascribed to a series of peaks shifted from the CuS covallite phase. The orange curve in **Figure 3c** shows the UV-Vis-NIR spectrum of the as-synthesized $Cu_{2-x}S$ NCs in trichloroethylene. The broad peak exhibiting maximal intensity at 1291 nm is attributed to the LSPR of $Cu_{2-x}S$ NCs based on the numerous holes generated from the self-doping effect, which is proportional to the number of copper-deficient sites in the crystal. $Cu_{2-x}S$ NCs with a higher hole density (*i.e.*, a larger $x$ value) yielded a more intense LSPR effect at a lower wavelength and vice versa for those with a lower hole density (*i.e.*, a smaller $x$ value).

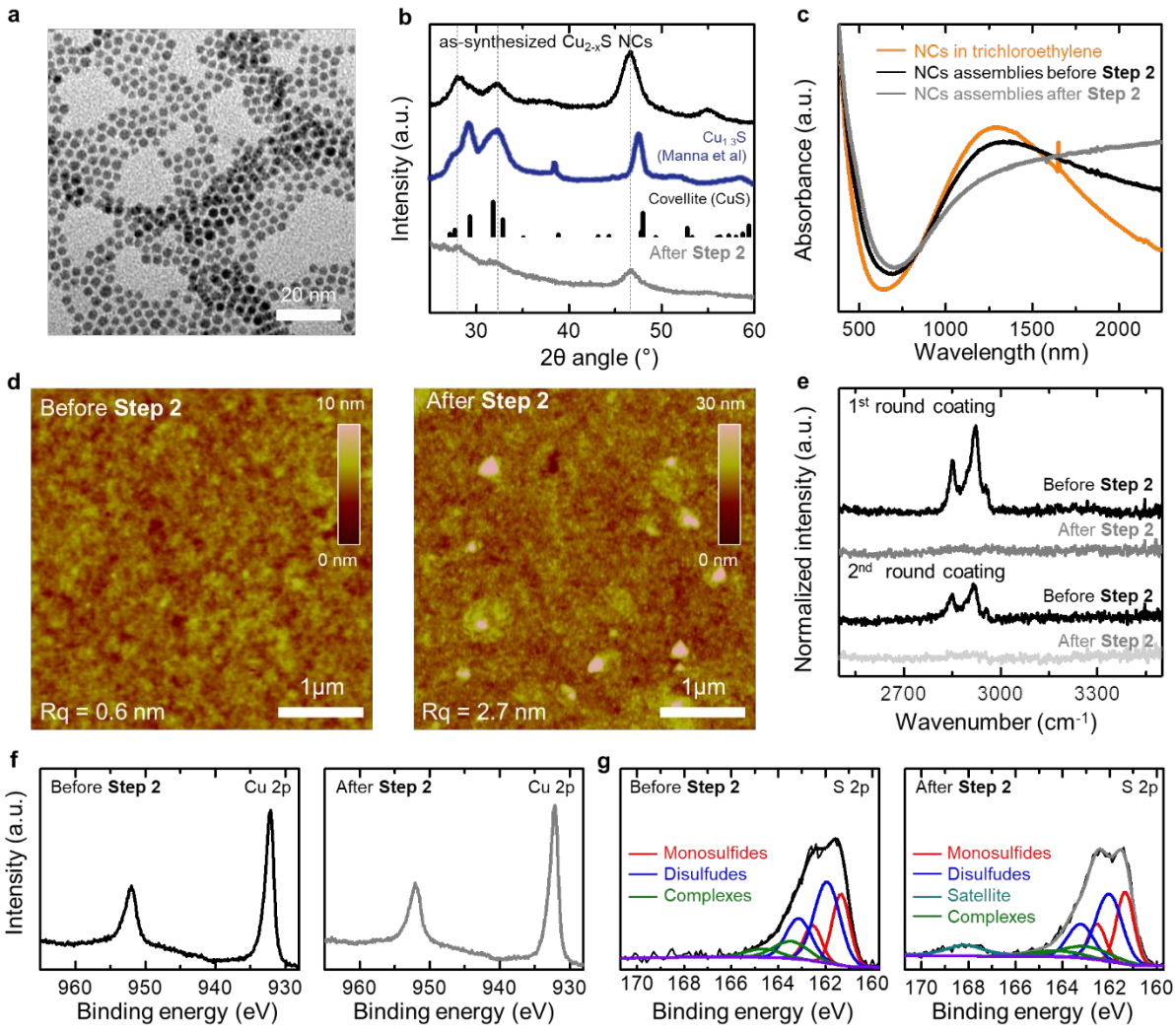


**Figure 3.** (a) TEM image of the as-synthesized $Cu_{2-x}S$ NCs. (b) X-ray diffractogram of the as-synthesized $Cu_{2-x}S$ NCs (black) and $Cu_{2-x}S$ NCs assemblies after Step 2 (gray), i.e., the ligand treatment step. (c) UV-Vis-NIR absorbance spectrum of $Cu_{2-x}S$ NCs in solution (orange) and in thin film assemblies before (black) and after (gray) treatment with $Na_2S$ solution. (d) AFM images of the as-prepared $Cu_{2-x}S$ NC film (left) and $Cu_{2-x}S$ NC film applied with secondary NC deposition (right). (e) FT-IR spectra of $Cu_{2-x}S$ NCs assemblies at different stages of the process. (f) High resolution Cu 2p XPS spectra for thin film assemblies of $Cu_{2-x}S$ NCs before (left) and after (right) treating with $Na_2S$ solution. (g) High resolution S 2p XPS spectra for thin film assemblies of $Cu_{2-x}S$ NCs before (left) and after (right) treating with $Na_2S$ solution. Deconvoluted subcomponents are displayed in colors.

Next, assemblies of $Cu_{2-x}S$ NCs were prepared by spin-coating a dispersion of NCs in a solvent mixture of hexane and toluene (3:7 volume ratio). The as-spin-coated NC films exhibited an insulating behavior due to the long oleylamine surrounding the individual NCs, indicating that each NC is weakly coupled with each other. The black curve in **Figure 3c** shows the UV-Vis-NIR spectrum of the film showing characteristic NIR LSPR absorbance. The morphology observed by atomic force microscopy (AFM) is shown in **Figure 3d** (left). To enhance the electronic coupling, a mixture of sodium sulfide ($Na_2S$) solution (0.064 M) in ethanol was dropped onto the $Cu_{2-x}S$ NC film, which was dwelled for 2 min before spinning. During this dwell time, the original oleylamine ligands were removed from the NC surface. The removal of oleylamine ligands was confirmed from a series of FT-IR spectra (**Figure 3e**). The peaks in the FT-IR spectra over the given range of wavenumbers between 2800 and 3000 $cm^{-1}$ can be assigned to the stretching vibration of the C-H bond, which is indicative of the original oleylamine ligands. The disappearance of these peaks in the FT-IR spectrum of the $Cu_{2-x}S$ NCs films indicates that the oleylamine ligands on the surface of $Cu_{2-x}S$ NCs were completely removed during the dwell time. Once the original oleylamine ligands were removed from the surface of NCs, enhanced coupling between the neighboring NCs, which yield finite film conductivity (see below), could be achieved. However, the enhancement did not remove the localization of the surface plasmon generated in the nanostructure. The characteristic NIR absorbance of the NC film remained but with significant broadening in the longer-wavelength regime. Owing to the reduced distance between the NCs after adjusting the original ligands, microscopic cracks were formed over the NC films, preventing the formation of a percolated pathway for charge carriers to transport. Therefore, we additionally spin-coated a dispersion of $Cu_{2-x}S$ NCs, in between the applications of the $Na_2S$ solution, to fill the cracks and form continuous films of highly coupled $Cu_{2-x}S$ NC assemblies. The right panel in **Figure 3d** shows the final AFM image of $Cu_{2-x}S$ NC assemblies without apparent cracks, which underwent additional NC deposition and subsequent $Na_2S$ treatment. The resulting assemblies of $Cu_{2-x}S$ NCs yielded a finite electrical conductivity of 349.8 $Scm^{-1}$, confirming that they were electronically coupled. The black spectra in **Figure 3e** are attributed to an assembly of $Cu_{2-x}S$ NCs ligated with oleylamine. The gray spectra are attributed to the assembly executed with the first round of $Na_2S$ treatment.

XPS measurements were conducted to examine the surface characteristics of the $Cu_{2-x}S$ NC assemblies. The sulfur content may be subjected to change since $S^{2-}$ from the treatment solution can be actively involved in the process. However, the overall composition between Cu and S remained unchanged after $Na_2S$ treatment (**Table 1**). This indicates that no additional sulfur was introduced into the $Cu_{2-x}S$ NCs during $Na_2S$ treatment. **Figure 3f** and **3g** shows the high-resolution Cu 2p and S 2p XPS spectra for $Cu_{2-x}S$ NC films, respectively, before (black) and after (gray) being treated with $Na_2S$ solution. Two peaks were observed at binding energies of 931 and 951 eV

for the $Cu_{2-x}S$ NC assemblies before and after treatment with the $Na_2S$ solution, which correspond to Cu $2p_{3/2}$ and Cu $2p_{1/2}$, respectively. Meanwhile, the characteristic satellite peak of the Cu(II) state at 943 eV was not observed for both films.[28] The results confirm that the oxidation state of the Cu element is +1 for both films. There are two different types of coordination for sulfur atoms contained in the covellite structure, comprising alternating layers of (i) CuS with copper atoms in planar trigonal coordination and (ii) $Cu_2S_2$ with copper atoms in tetrahedral coordination (an extended chemical formula of $(Cu^+)_3(S^{2-})(S\text{-}S)^-$ is often used for covellites).[11] Considering that the given $Cu_{2-x}S$ NCs exist in the covellite phase, the chemical formula of $Cu_{2-x}S$ NCs can be expressed as $(Cu^+)_{2-3y}(S^{2-})_{1-2y}(S\text{-}S)_y^-$ (where $y = x/3$). Thus, the S 2p spectra for the $Cu_{2-x}S$ NCs could be deconvoluted into subcomponents, including the peak arising from disulfide (162.1 and 163.3 eV, blue curves in the spectrum) and monosulfide (161.4 and 162.6 eV, red curves in the spectrum) moieties. Upon $Na_2S$ treatment, the relative intensity of the subcomponent peaks corresponding to those of the disulfides decreased. Although the overall composition of the $Cu_{2-x}S$ NCs remains invariant upon the treatment, a new broad peak also appeared upon $Na_2S$ treatment at a binding energy of 168.2 eV, We assign this peak to sulfur on the NC surface absorbed with oxygen[29-30] perhaps from the ethanol solvent we used in $Na_2S$ solution (this peak disappears after Step 3 below).

**Table 1.** Summary of the areal intensity obtained for subcomponents of high-resolution S 2p spectra for assemblies of $Cu_{2-x}S$ NCs prepared under different conditions.

| | Chemical | Immersion time | $x$ | Monosulfide (%) | Disulfide (%) | Complexes (%) | Satellite (%) |
|---|---|---|---|---|---|---|---|
| before Step 2 | - | | 0.9 | 32.0 | 52.9 | 15.1 | |
| after Step 2 | Cu(I) complex | 0 | 0.9 | 31.8 | 45.0 | 15.2 | 8.0 |
| Step 3 | Cu(I) complex | 1 | 0.5 | 55.2 | 29.6 | 15.2 | |
| Step 3 | Cu(I) complex | 5 | 0.2 | 73.1 | 11.7 | 15.2 | |
| Step 3′ | Cu(I) and Ce(IV) complex | 5, 1 | 0.4 | 61.9 | 22.9 | 15.1 | |
| Step 3′ | Cu(I) and Ce(IV) complex | 5, 6 | 0.7 | 46.7 | 38.1 | 15.1 | |
| Step 3′ | Cu(I) and Ce(IV) complex | 5, 11 | 0.9 | 31.0 | 53.9 | 15.1 | |

Once the as-prepared highly coupled assemblies of $Cu_{2-x}S$ NCs were formed, the stoichiometric doping was conducted by immersing the assemblies into a solution containing tetrakis copper hexafluorophosphate ($Cu(CH_3CN)_4PF_6$) for various periods of time (Step 3 in **Figure 1**). Exposing $Cu(CH_3CN)_4PF_6$ to $Cu_{2-x}S$ NCs in solution supplies $Cu^+$ to the nanocrystal, which can be inserted

into the copper-deficient sites.[9, 11] We anticipate the same effect for our assemblies of $Cu_{2-x}S$ NCs. While the stoichiometry modification done by the chemical approaches for $Cu_{2-x}S$ NCs in solution have been reported and the resulting optical and structural properties of materials in solution have been explored previously, very few studies have actually gone beyond the material characterization in solution phase and have attempted the chemical approaches to solid state NC assemblies.

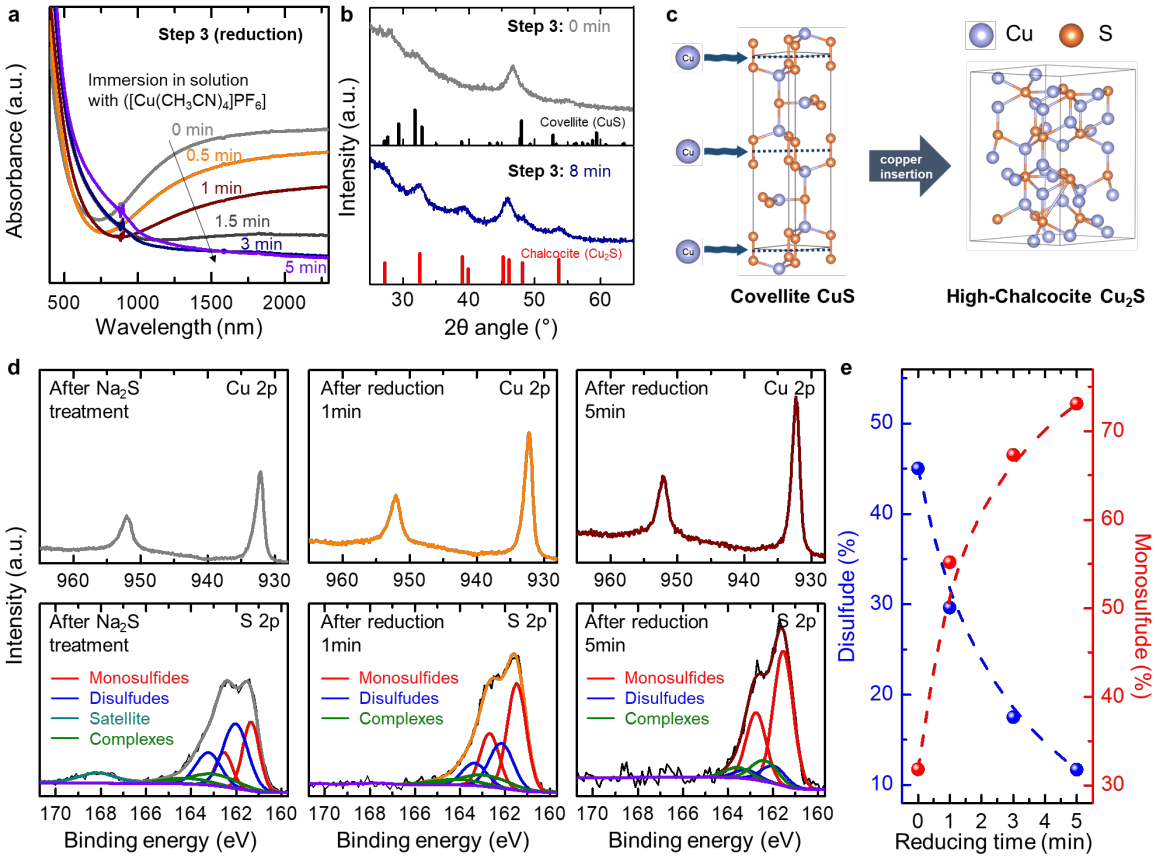


**Figure 4.** (a) UV-Vis-NIR absorbance spectrum of highly coupled $Cu_{2-x}S$ NCs assemblies treated with $[Cu(CH_3CN)_4]PF_6$ solution. (b) X-ray diffractograms of highly coupled $Cu_{2-x}S$ NCs assemblies treated with $[Cu(CH_3CN)_4]PF_6$ solution. (c) Schematic description of transition of $Cu_{2-x}S$ NCs from covellite phase to chalcocite phase upon insertion of copper. (d) High resolution Cu 2p XPS and S 2p XPS spectra for highly coupled $Cu_{2-x}S$ NCs assemblies treated with $[Cu(CH_3CN)_4]PF_6$ solution. (e) Relative of sulfur elements in disulfide and monosulfide forms for highly coupled $Cu_{2-x}S$ NCs assemblies treated with $[Cu(CH_3CN)_4]PF_6$ solution

**Figure 4a** shows the UV-Vis-NIR spectra of the highly coupled assemblies of $Cu_{2-x}S$ NCs treated with 1 mM of $Cu(CH_3CN)_4PF_6$ in methanol for different time periods (0, 0.5, 1, 1.5, 3, and

5 min). As the immersion time increased, the NIR absorbance of the film ascribed to the LSPR effect decreased gradually, indicating that the density of holes in the assemblies of $Cu_{2-x}S$ NCs decreased. The decreased density of holes can be attributed to the insertion of $Cu^+$ (from the solution with $Cu(CH_3CN)_4PF_6$) into the copper vacant sites within the assemblies of $Cu_{2-x}S$ NCs. In fact, the composition of copper and sulfur obtained from XPS analysis gradually changed from 1.1:1 (*i.e.*, $x = 0.9$) to 1.8:1 (*i.e.*, $x = 0.2$) by immersing the film in the $Cu^+$ solution for 5 min (**Table 1**).

The structural analysis of the assemblies led to a detailed understanding of the effect of $Cu^+$. **Figure 4b** shows the X-ray diffractograms of the $Cu_{2-x}S$ NC assemblies collected before (gray) and after (navy) treating the film with Cu(I) complex solution for an adequate amount of time (8 min), leading to a complete disappearance of the NIR absorbance from the LSPR effect. The diffractogram of the original electronically coupled $Cu_{2-x}S$ NC assemblies, corresponding to the covellite phase with a negative peak shift towards a lower $2\theta$ angle, evolved into that corresponding to the chalcocite phase characterized by two distinct peaks at 39.0° and 39.9° after adequately treating the film with the Cu(I) complex solution. This is consistent with the result reported by Manna et al,[11] who conducted $Cu(CH_3CN)_4PF_6$ treatment on $Cu_{2-x}S$ NCs in solution; in their study, the peaks assigned to the covellite phase gradually shifted towards a lower $2\theta$ angle as more $Cu^+$ ions were incorporated into the NCs and eventually transitioned into the chalcocite phase. It is suggested that $Cu^+$ inserted into covellite may lead to cleavage of the disulfides and newly generated monosulfides, leading the covellite structure to eventually evolve into chalcocite (**Figure 4c**).[31-32] Consistent with this scenario, the relative areal intensity of the deconvoluted subcomponent peaks in the S 2p spectra from XPS measurements between the disulfide and monosulfide peaks changed with time (**Figure 4d**). **Figure 4e** summarizes the relative composition of sulfur elements in disulfide and monosulfide forms; the percentage of monosulfides increased while that of disulfides decreased as the immersion time in the $Cu^+$ solution increased.

In contrast, the suppressed LSPR absorbance of highly coupled $Cu_{2-x}S$ NC assemblies could be recovered by immersing the film into a new solution containing cerium ammonium nitrate ($(NH_4)_2Ce(NO_3)_6$), an oxidizing agent that extracts copper from $Cu_{2-x}S$ NCs (**Figure 5a**). **Figure 5b** shows the UV-Vis-NIR spectrum of the highly coupled $Cu_{2-x}S$ NC assemblies that were initially treated with the ($Cu(CH_3CN)_4PF_6$) solution for 5 min, followed by subsequent treatment with 0.4 mM of $(NH_4)_2Ce(NO_3)_6$ in ethanol for 11 min. As the immersion time in the Ce(IV) complex solution increased, the LSPR absorbance reappeared and its intensity gradually increased, indicating that the density of holes in the $Cu_{2-x}S$ NC assemblies increased. In fact, after oxidative treatment (11 min) of the $Cu_{2-x}S$ NC assemblies, which had already undergone reductive treatment in $Cu(CH_3CN)_4PF_6$ for 5 min, the shape of the UV-Vis-NIR spectrum recovered to that achieved

from original $Cu_{2-x}S$ NC assemblies prior to reductive treatment. In addition, the $x$ value of the $Cu_{2-x}S$ NCs estimated from XPS measurements recovered its original value (*i.e.*, $x = 0.9$), and the diffraction pattern recovered its original shape (**Figure 5c**). **Figure 5d** shows a series of high-resolution Cu 2p and S 2p XPS spectra for $Cu_{2-x}S$ NC assemblies immersed in $(NH_4)_2Ce(NO_3)_6$ solution for different periods of time. As the immersion time increases, the relative areal intensity of the deconvoluted subcomponent peaks in the S 2p spectra from XPS measurements between the disulfide peaks increased compared to that of the monosulfide peaks (**Figure 5e**), exhibiting a completely opposite behavior to that shown in **Figure 4e**.

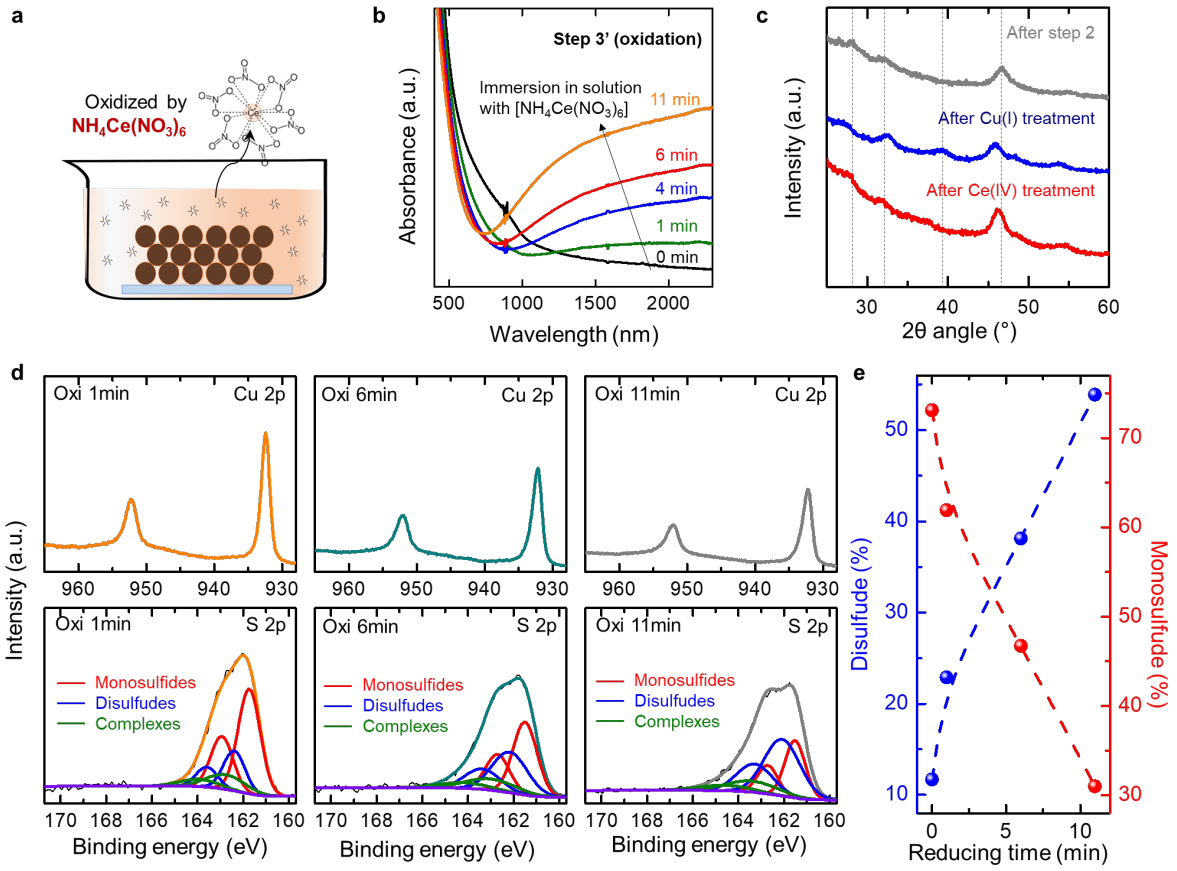


**Figure 5.** (a) Schematic description of the $(NH_4)_2Ce(NO_3)_6$ treatment process on highly coupled assemblies of $Cu_{2-x}S$ NCs. (b) UV-Vis-NIR absorbance spectrum of highly coupled $Cu_{2-x}S$ NCs assemblies treated with $(NH_4)_2Ce(NO_3)_6$ solution. (c) X-ray diffractograms of highly coupled $Cu_{2-x}S$ NC assemblies treated with $[Cu(CH_3CN)_4]PF_6$ and $(NH_4)_2Ce(NO_3)_6$ solution. (d) High resolution Cu 2p XPS and S 2p XPS spectra for highly coupled $Cu_{2-x}S$ NCs assemblies treated

with $(NH_4)_2Ce(NO_3)_6$ solution. (e) Relative sulfur elements in disulfide and monosulfide forms for highly coupled $Cu_{2-x}S$ NC assemblies treated with $(NH_4)_2Ce(NO_3)_6$ solution.

The electrical and thermoelectrical characteristics of these $Cu_{2-x}S$ NC assemblies with controlled stoichiometry were examined at room temperature. This was achieved using a four-probe electrical measurement coupled with two Peltier devices that generated a temperature gradient across the $Cu_{2-x}S$ NC assemblies (**Figure 6a**). Compared to the films of $Cu_{2-x}S$ NCs with original oleylamine ligands, the electrical conductivity of the films treated with $Na_2S$ solution increased significantly. It should be noted that the sheet resistance of the $Cu_{2-x}S$ NC films with original oleylamine ligands exceeded the measurable limitation. The conductivity ($\sigma$) of the electronically coupled $Cu_{2-x}S$ NC films is represented by black circles in **Figure 6b**, plotted as a function of the immersion time in the Cu(I) complex solution, which resulted in a gradual change in $x$. With more amount of $Cu^+$ incorporated into the $Cu_{2-x}S$ NCs, the conductivity of the film gradually decreased. For assemblies of $Cu_{2-x}S$ NC films with $x = 0.9$, $\sigma = 349.8$ $Scm^{-1}$. This value became 32.6 and 28.0 $Scm^{-1}$ as $x$ was reduced to 0.2 and 0.1, respectively. We attribute the decrease in conductivity to the reduced density of holes upon immersing the film in the $Cu^+$ solution, which was independently confirmed from the UV-Vis-NIR spectrum of the film with lowered LSPR absorbance (**Figure 3a**).

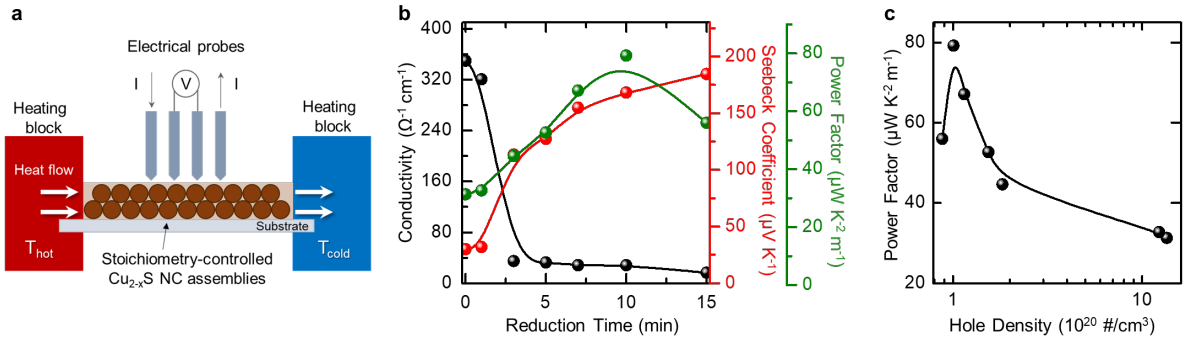


**Figure 6.** (a) Schematic description of the thermoelectric measurement of highly coupled assemblies of $Cu_{2-x}S$ NCs. (b) Conductivity (black), Seebeck coefficient (red), and power factor (green) of highly coupled assemblies of $Cu_{2-x}S$ NCs plotted as a function of the immersion time of the film in the $Cu^+$ solution. The values of $x$ for the given $Cu_{2-x}S$ NC assemblies are also depicted in the plot. (c) Power factor of highly coupled assemblies of $Cu_{2-x}S$ NCs plotted as a function of the hole density of the film.

From the thermoelectrical measurements over a small temperature difference of ±2 K at room temperature, positive Seebeck coefficients ($S$) were obtained for the entire series of samples, indicating that holes are mainly involved in the transport through films of $Cu_{2-x}S$ NCs. We attribute this thermoelectric effect mainly to the electronic Seebeck effect based on holes rather than to the

ionic Seebeck effect based on diffusive $Cu^{+}$. In contrast to $\sigma$, $S$ increased as the immersion time of the film in the Cu(I) complex solution (the red circles in **Figure 6b**) increased. Typically, decreasing the charge density involved in thermoelectric transport enhances the Seebeck voltage generated from the given material.[33-37] The immersion of electronically coupled $Cu_{2-x}S$ NC films in the Cu(I) complex solution, which result in a lower density of holes ($p$) in $Cu_{2-x}S$ NCs, yielded a consistent effect. The green circles in **Figure 6b** show the power factor ($P$) of the $Cu_{2-x}S$ NC assemblies, which is equal to $\sigma S^2$. Since $\sigma$ and $S$ vary oppositely with the carrier concentration ($\sigma$ increases with $p$, while $S$ decreases with $p$), a maximum power factor of 79.2 $\mu W\ K^{-2}m^{-1}$ was obtained at an optimal stoichiometry of $x = 0.1$ in highly coupled assemblies of $Cu_{2-x}S$ NCs. Quantitatively, we could estimate the density of the holes from the Seebeck coefficient using the relation $S = (8\pi^2 k_B^2/3eh^2)m_h T(\pi/3p)^{2/3}$, where $k_B$ is the Boltzmann constant, $e$ is the elemental charge, $h$ is the Planck constant, and $m_h$ is the effective hole mass of the material (1.8 $m_0$).[38] **Figure 6c** shows the power factor as a function of the as-estimated hole density. To the best of our knowledge, the results show, for the first time, the power factor vs. carrier density relation obtained at room temperature for $Cu_{2-x}S$ NCs based thermoelectric systems with delicate hole density control. The results are summarized in **Table 2**.

**Table 2.** Summary of the electrical conductivity, Seebeck coefficient, power factor, and hole densities for assemblies of $Cu_{2-x}S$ NCs with different values of $x$.

| Immersion time (min) | $x$ | Electrical conductivity ($\Omega^{-1}cm^{-1}$) | Seebeck coefficient ($\mu V\ K^{-1}$) | Power factor ($\mu W\ K^{-2}m^{-1}$) | Hole density ($10^{20}$ # $cm^{-3}$) |
|---|---|---|---|---|---|
| 0 | 0.9 | 349.8 | 29.9 | 31.3 | 13.5 |
| 1 | 0.5 | 320.8 | 31.9 | 32.7 | 12.3 |
| 3 | 0.3 | 34.7 | 113.4 | 44.6 | 1.83 |
| 5 | 0.2 | 32.6 | 127.2 | 52.7 | 1.54 |
| 7 | - | 28.0 | 154.7 | 67.1 | 1.15 |
| 10 | 0.1 | 28.0 | 168.3 | 79.2 | 1.01 |

## 5.0 CONCLUSION

We report the influence of stochiometric doping on the structural, optical, electrical, and thermoelectric properties of highly coupled $Cu_{2-x}S$ NC thin film assemblies. The core of the doping

relied on controlling the atomic stoichiometric mismatch of the material, *i.e.*, *x*, ranging from 0.9 to 0.1. This was accomplished by chemically treating the highly coupled $Cu_{2-x}S$ NC assemblies that supply or extract $Cu^+$ into or from the nanocrystal lattice, respectively. As $Cu^+$ occupied the copper-deficient sites of $Cu_{2-x}S$ NCs, the NIR absorbance of the $Cu_{2-x}S$ NC assemblies as well as their electrical conductivity and thermoelectric Seebeck coefficient changed systematically. The $Cu_{2-x}S$ NC assemblies capable of delicately controlling the carrier density provide an excellent material platform for investing the fundamental characteristics of nanostructured systems e.g., the charge transport mechanism through NC assemblies. Further, controlling the physical characteristics of $Cu_{2-x}S$ NC assemblies also provide practical guidelines for exploiting this emerging class of nanocrystal system based on doping for example as Fermi level-controlled hole transport layer[39-40] and wavelength-tailored plasmonic layer[1, 41-42] in optoelectronic devices, or as defect-controlled electrocatalyst and photocatalysts[43-44] .

## 6.0 REFERENCES


(1) Coughlan, C.; Ibanez, M.; Dobrozhan, O.; Singh, A.; Cabot, A.; Ryan, K. M., Comp ound Copper Chalcogenide Nanocrystals. *Chem. Rev.* **2017,** *117* (9), 5865-6109.

(2) Liu, X.; Wang, X. L.; Zhou, B.; Law, W. C.; Cartwright, A. N.; Swihart, M. T., Siz e-Controlled Synthesis of $Cu_{2-x}E$ (E = S, Se) Nanocrystals with Strong Tunable Near-Infr ared Localized Surface Plasmon Resonance and High Conductivity in Thin Films. *Adv. F unct. Mater.* **2013,** *23* (10), 1256-1264.

(3) Luther, J. M.; Jain, P. K.; Ewers, T.; Alivisatos, A. P., Localized Surface Plasmon R esonances Arising from Free Carriers in Doped Quantum Dots. *Nat. Mater.* **2011,** *10* (5), 361-366.

(4) Hsu, S. W.; Ngo, C.; Tao, A. R., Tunable and Directional Plasmonic Coupling withi n Semiconductor Nanodisk Assemblies. *Nano Lett.* **2014,** *14* (5), 2372-2380.

(5) Willets, K. A.; Van Duyne, R. P., Localized Surface Plasmon Resonance Spectroscop y and Sensing. *Annu. Rev. Phys. Chem.* **2007,** *58*, 267-297.

(6) Link, S.; El-Sayed, M. A., Spectral Properties and Relaxation Dynamics of Surface P lasmon Electronic Oscillations in Gold and Silver Nanodots and Nanorods. *J. Phys. Che m. B* **1999,** *103* (40), 8410-8426.

(7) Kriegel, I.; Scotognella, F.; Manna, L., Plasmonic Doped Semiconductor Nanocrystals: Properties, Fabrication, Applications and Perspectives. *Phys. Rep.* **2017,** *674*, 1-52.

(8) Mattox, T. M.; Ye, X. C.; Manthiram, K.; Schuck, P. J.; Alivisatos, A. P.; Urban, J. J., Chemical Control of Plasmons in Metal Chalcogenide and Metal Oxide Nanostructure s. *Adv. Mater.* **2015,** *27* (38), 5830-5837.

(9) Dorfs, D.; Hartling, T.; Miszta, K.; Bigall, N. C.; Kim, M. R.; Genovese, A.; Falqui, A.; Povia, M.; Manna, L., Reversible Tunability of the Near-Infrared Valence Band Plas mon Resonance in $Cu_{2-x}Se$ Nanocrystals. *J. Am. Chem. Soc.* **2011,** *133* (29), 11175-11180 .

(10) Jain, P. K.; Manthiram, K.; Engel, J. H.; White, S. L.; Faucheaux, J. A.; Alivisatos,

A. P., Doped Nanocrystals as Plasmonic Probes of Redox Chemistry. *Angew. Chem. Int. Ed.* **2013,** *52* (51), 13671-13675.
(11) Xie, Y.; Riedinger, A.; Prato, M.; Casu, A.; Genovese, A.; Guardia, P.; Sottini, S.; Sangregorio, C.; Miszta, K.; Ghosh, S.; Pellegrino, T.; Manna, L., Copper Sulfide Nanocrystals with Tunable Composition by Reduction of Covellite Nanocrystals with $Cu^{+}$ Ions. *J. Am. Chem. Soc.* **2013,** *135* (46), 17630-17637.
(12) Kriegel, I.; Jiang, C. Y.; Rodriguez-Fernandez, J.; Schaller, R. D.; Talapin, D. V.; da Como, E.; Feldmann, J., Tuning the Excitonic and Plasmonic Properties of Copper Chalcogenide Nanocrystals. *J. Am. Chem. Soc.* **2012,** *134* (3), 1583-1590.
(13) Patel, T. A.; Panda, E., Copper Deficiency Induced Varying Electronic Structure and Optoelectronic Properties of $Cu_{2-x}S$ Thin Films. *Appl. Surf. Sci.* **2019,** *488*, 477-484.
(14) He, Y.; Day, T.; Zhang, T.; Liu, H.; Shi, X.; Chen, L.; Snyder, G. J., High Thermoelectric Performance in Non-Toxic Earth-Abundant Copper Sulfide. *Adv. Mater.* **2014,** *26* (23), 3974-3978.
(15) Liu, Y.; Gibbs, M.; Puthussery, J.; Gaik, S.; Ihly, R.; Hillhouse, H. W.; Law, M., Dependence of Carrier Mobility on Nanocrystal Size and Ligand Length in PbSe Nanocrystal Solids. *Nano Lett.* **2010,** *10* (5), 1960-1969.
(16) Talapin, D. V.; Murray, C. B., PbSe Nanocrystal Solids for n- and p-channel Thin Film Field-effect Transistors. *Science* **2005,** *310* (5745), 86-89.
(17) Otelaja, O. O.; Ha, D. H.; Ly, T.; Zhang, H. T.; Robinson, R. D., Highly Conductive $Cu_{2-x}S$ Nanoparticle Films through Room-Temperature Processing and an Order of Magnitude Enhancement of Conductivity via Electrophoretic Deposition. *ACS Appl. Mater. Interfaces* **2014,** *6* (21), 18911-18920.
(18) Dibenedetto, C. N.; Fanizza, E.; Brescia, R.; Kolodny, Y.; Remennik, S.; Panniello, A.; Depalo, N.; Yochelis, S.; Comparelli, R.; Agostiano, A.; Curri, M. L.; Paltiel, Y.; Striccoli, M., Coupling Effects in QD Dimers at Sub-nanometer Interparticle Distance. *Nano Res.* **2020,** *13* (4), 1071-1080.
(19) Samadi Khoshkhoo, M.; Lox, J. F. L.; Koitzsch, A.; Lesny, H.; Joseph, Y.; Lesnyak, V.; Eychmüller, A., Highly Conductive Copper Selenide Nanocrystal Thin Films for Advanced Electronics. *ACS Appl. Electron. Mater.* **2019,** *1* (8), 1560-1569.
(20) Gao, Y. N.; Aerts, M.; Sandeep, C. S. S.; Talgorn, E.; Savenije, T. J.; Kinge, S.; Siebbeles, L. D. A.; Houtepen, A. J., Photoconductivity of PbSe Quantum-Dot Solids: Dependence on Ligand Anchor Group and Length. *ACS Nano* **2012,** *6* (11), 9606-9614.
(21) Yun, H. J.; Paik, T.; Edley, M. E.; Baxter, J. B.; Murray, C. B., Enhanced Charge Transfer Kinetics of CdSe Quantum Dot-Sensitized Solar Cell by Inorganic Ligand Exchange Treatments. *ACS Appl. Mater. Interfaces* **2014,** *6* (5), 3721-3728.
(22) Luther, J. M.; Law, M.; Song, Q.; Perkins, C. L.; Beard, M. C.; Nozik, A. J., Structural, Optical and Electrical Properties of Self-assembled Films of PbSe Nanocrystals Treated with 1,2-ethanedithiol. *ACS Nano* **2008,** *2* (2), 271-280.
(23) Zhang, H.; Jang, J.; Liu, W. Y.; Talapin, D. V., Colloidal Nanocrystals with Inorganic Halide, Pseudohalide, and Halometallate Ligands. *ACS Nano* **2014,** *8* (7), 7359-7369.
(24) Lee, J.; Gim, Y.; Yang, J.; Jo, H.; Han, J.; Lee, H.; Kim, D. H.; Huh, W.; Cho, J.

H.; Kang, M. S., Graphene Phototransistors Sensitized by $Cu_{2-x}Se$ Nanocrystals with Sho rt Amine Ligands. *J. Phys. Chem. C* **2017,** *121* (9), 5436-5443.
(25) Nag, A.; Kovalenko, M. V.; Lee, J. S.; Liu, W. Y.; Spokoyny, B.; Talapin, D. V., Metal-free Inorganic Ligands for Colloidal Nanocrystals: $S^{2-}$, $HS^-$, $Se^{2-}$, $HSe^-$, $Te^{2-}$, $HTe^-$, $TeS_3^{2-}$, $OH^-$, and $NH_2^-$ as Surface Ligands. *J. Am. Chem. Soc.* **2011,** *133* (27), 10612-10 620.
(26) Lee, J.; Yang, J.; Park, C.; Kim, J. H.; Kang, M. S., Electronic Properties of $Cu_{2-x}$ Se Nanocrystal Thin Films Treated with Short Ligand ($S_2^-$, $SCN^-$, and $Cl^-$) Solutions. *J. Phys. Chem. C* **2016,** *120* (27), 14899-14905.
(27) Balitskii, O. A.; Sytnyk, M.; Stangl, J.; Primetzhofer, D.; Groiss, H.; Heiss, W., Tu ning the Localized Surface Plasmon Resonance in $Cu_{2-x}Se$ Nanocrystals by Postsynthetic Ligand Exchange. *ACS Appl. Mater. Interfaces* **2014,** *6* (20), 17770-17775.
(28) Ma, M.; Djanashvili, K.; Smith, W. A., Selective Electrochemical Reduction of $CO_2$ to CO on CuO-derived Cu Nanowires. *Phys. Chem. Chem. Phys.* **2015,** *17* (32), 20861-2 0867.
(29) Czioska, S.; Wang, J.; Teng, X.; Chen, Z., Hierarchically Structured $CuCo_2S_4$ Nano wire Arrays as Efficient Bifunctional Electrocatalyst for Overall Water Splitting. *ACS Sus tain. Chem. Eng.* **2018,** *6* (9), 11877-11883.
(30) Chandra Deb Nath, N.; Yoo, K.; Lee, J.-J., Halogen-Free Guanidinium-based Perovs kite Solar Cell with Enhanced Stability. *RSC Adv.* **2018,** *8* (31), 17365-17372.
(31) Fjellvåg, H.; Grønvold, F.; Stølen, S.; Andresen, A.; Müller-Käfer, R., Low-temperat ure Structural Distortion in CuS. *Z. Kristallogr. Cryst. Mater.* **1988,** *184*, 111-121.
(32) Buerger, M. J.; Wuensch, B. J., Distribution of Atoms in High Chalcocite, $Cu_2S$. *Sc ience* **1963,** *141* (3577), 276-277.
(33) Venkateshvaran, D.; Nikolka, M.; Sadhanala, A.; Lemaur, V.; Zelazny, M.; Kepa, M .; Hurhangee, M.; Kronemeijer, A. J.; Pecunia, V.; Nasrallah, I.; Romanov, I.; Broch, K.; McCulloch, I.; Emin, D.; Olivier, Y.; Cornil, J.; Beljonne, D.; Sirringhaus, H., Approach ing Disorder-free Transport in High-mobility Conjugated Polymers. *Nature* **2014,** *515* (75 27), 384-388.
(34) Bubnova, O.; Khan, Z. U.; Malti, A.; Braun, S.; Fahlman, M.; Berggren, M.; Crispi n, X., Optimization of the Thermoelectric Figure of Merit in the Conducting Polymer Pol y(3,4-ethylenedioxythiophene). *Nat. Mater.* **2011,** *10* (6), 429-433.
(35) Zhao, L.-D.; Hao, S.; Lo, S.-H.; Wu, C.-I.; Zhou, X.; Lee, Y.; Li, H.; Biswas, K.; Hogan, T. P.; Uher, C.; Wolverton, C.; Dravid, V. P.; Kanatzidis, M. G., High Thermoel ectric Performance via Hierarchical Compositionally Alloyed Nanostructures. *J. Am. Chem . Soc.* **2013,** *135* (19), 7364-7370.
(36) Scimeca, M. R.; Yang, F.; Zaia, E.; Chen, N.; Zhao, P.; Gordon, M. P.; Forster, J. D.; Liu, Y.-S.; Guo, J.; Urban, J. J.; Sahu, A., Rapid Stoichiometry Control in $Cu_2Se$ Th in Films for Room-Temperature Power Factor Improvement. *ACS Appl. Energy Mater.* **20 19,** *2* (2), 1517-1525.
(37) Kunpeng, Z.; Guan, M.; Qiu, P.; Blichfeld, A.; Eikeland, E.; Zhu, C.; Ren, D.; Xu, F.; Iversen, B.; Shi, X.; Chen, L., Thermoelectric Properties of $Cu_2Se_{1-x}Te_x$ Solid Solutio

ns. *J. Mater. Chem. A* **2018,** *6*.
(38) *Copper Sulfides ($Cu_2S$, $Cu_{2-x}S$) Energy Gap, Effective Masses: Datasheet from Landolt-Börnstein - Group III Condensed Matter · Volume 41C: "Non-Tetrahedrally Bonded Elements and Binary Compounds I" in SpringerMaterials (https://doi.org/10.1007/10681727_71)*, Springer-Verlag Berlin Heidelberg.
(39) Liu, L.; Zhou, B.; Deng, L.; Fu, W.; Zhang, J.; Wu, M.; Zhang, W.; Zou, B.; Zhong, H., Thermal Annealing Effects of Plasmonic $Cu_{1.8}S$ Nanocrystal Films and Their Photovoltaic Properties. *J. Phys. Chem. C* **2014,** *118* (46), 26964-26972.
(40) Tirado, J.; Roldán-Carmona, C.; Muñoz-Guerrero, F. A.; Bonilla-Arboleda, G.; Ralaiarisoa, M.; Grancini, G.; Queloz, V. I. E.; Koch, N.; Nazeeruddin, M. K.; Jaramillo, F., Copper Sulfide Nanoparticles as Hole-transporting-material in a Fully-inorganic Blocking Layers n-i-p Perovskite Solar Cells: Application and Working Insights. *Appl. Surf. Sci.* **2019,** *478*, 607-614.
(41) Zhao, Y.; Burda, C., Development of Plasmonic Semiconductor Nanomaterials with Copper Chalcogenides for a Future with Sustainable Energy Materials. *Energy. Environ. Sci.* **2012,** *5* (2), 5564-5576.
(42) Balitskii, O. A., Recent Energy Targeted Applications of Localized Surface Plasmon Resonance Semiconductor Nanocrystals: A Mini-review. *Mater. Today Energy* **2021,** *20*, 100629.
(43) Sun, S.; Li, P.; Liang, S.; Yang, Z., Diversified Copper Sulfide ($Cu_{2-x}S$) Micro-/Nanostructures: A Comprehensive Review on Synthesis, Modifications and Applications. *Nanoscale* **2017,** *9* (32), 11357-11404.
(44) Chen, L.; Hu, H.; Chen, Y.; Gao, J.; Li, G., Plasmonic $Cu_{2-x}S$ Nanoparticles: A Brief Introduction of Optical Properties and Applications. *Mater. Adv.* **2021,** *2* (3), 907-926.

## NOTICE AND SIGNATURE PAGE

Using Government drawings, specifications, or other data included in this document for any purpose other than Government procurement does not in any way obligate the U.S. Government. The fact that the Government formulated or supplied the drawings, specifications, or other data does not license the holder or any other person or corporation; or convey any rights or permission to manufacture, use, or sell any patented invention that may relate to them. This report is the result of contracted fundamental research deemed exempt from public affairs security and policy review in accordance with SAF/AQR memorandum dated 10 Dec 08 and AFRL/CA policy clarification memorandum dated 16 Jan 09. This report is available to the general public, including foreign nationals. Copies may be obtained from the Defense Technical Information Center (DTIC) (http://www.dtic.mil). FA2386-18-1-4008 HAS BEEN REVIEWED AND IS APPROVED FOR PUBLICATION.